Scalable Entanglement
of Trapped Ions

C. Monroe, C.A. Sackett, D. Kielpinski, B.E. King,
C. Langer, V. Meyer, C.J. Myatt, M. Rowe,
Q.A. Turchette, W.M. Itano, and D.J. Wineland

Time and Frequency Division, National Institute of Standards and Technology [1]
Boulder Colorado 80303

Abstract. Entangled states are both a crucial component in quantum computers, and of great interest in their own right, highlighting the inherent nonlocality of quantum mechanics. As part of the drive toward larger entangled states for quantum computing, we have engineered the most complex entangled state so far in a collection of four trapped atomic ions. Notably, we employ a technique that is readily scalable to much larger numbers of atoms. Limits to the current experiment and plans to circumvent these limitations are presented.

INTRODUCTION

At the heart of quantum mechanics lies the principle of superposition, where physical properties of a system can exist in two or more states simultaneously. When a system is composed of more than one degree of freedom, superpositions can be prepared where distinct degrees of freedom are perfectly correlated, yet the state of each degree of freedom is by itself in superposition. The prototypical example is Bohm's version [1] of the Einstein-Podolsky-Rosen paradox [2], where a spin-zero particle decays into a pair of spin-1/2 daughters, resulting in the singlet state

$$|\Psi_{EPR}\rangle = \frac{|\uparrow\rangle_1|\downarrow\rangle_2 - |\downarrow\rangle_1|\uparrow\rangle_2}{\sqrt{2}}. \tag{1}$$

This state is *entangled*, since it cannot be expressed as a direct product of states representing each particle. When one of the subsystems in such a state is measured,

the other subsystem is also determined, even when the particles are not in physical contact or outside each other's light cones. In general, entangled states such as $|\Psi_{EPR}\rangle$ highlight the nonlocal character of quantum mechanics. Quantitatively, this is usually expressed in terms of a violations of Bell's inequality [3], where measured correlations between the entangled subsystems can be shown to be incompatible with what would be expected under conditions of local realism.

Although the correlation in the above state cannot be used for superluminal communication, it can be harnessed for enhancing communication rates over what can be obtained classically [4,5]. Furthermore, such states are useful in a variety of quantum communication schemes such as quantum cryptography [6] and quantum "teleportation" [7–10].

Entangled states of larger systems are a defining feature of a quantum computer. Here, for example, a collection of N spin-1/2 particles are prepared in an arbitrary entangled state of the form

$$|\Psi_{QC}\rangle = a_0|000\ldots0\rangle + a_1|000\ldots1\rangle + \ldots + a_{2^N-1}|111\ldots1\rangle, \qquad (2)$$

where $|0\rangle$ and $|1\rangle$ refer to the two spin states of each particle, and the a_k are the amplitudes of the number k being stored by the register of particles. By choosing appropriate entangled states and performing appropriate state measurements of the particles, quantum computers can solve certain problems much faster than any classical computer [11,12]. The reason quantum computers are mere speculation at this point is that $|\Psi_{QC}\rangle$ is very difficult to produce in the laboratory.

SCALABLE ENTANGLEMENT WITH TRAPPED IONS

Nearly every demonstration of entanglement to date has relied upon a random or selection process that prohibits scaling to large numbers of particles. This can be quantified in terms of the *entanglement efficiency* parameter ϵ, or the probability per unit time that a perfectly entangled pair is created [13]. The probability of realizing a perfect N-particle entangled state typically scales as ϵ^{cN}, where c is of order unity and depends on the particular experiment.

The first measured violations of Bell's inequality were seen in atomic cascade experiments involving the entanglement of a pair of spontaneously emitted photons [14,15]. Spontaneous parametric downconversion is now a popular source of entangled photons, where typically ultraviolet photons traverse a nonlinear crystal and downconvert into a pair of polarization-entangled infrared beams [16,17]. Unfortunately, the probability of each input photon being converted leads to an efficiency $\epsilon \simeq 10^{-4}$, so the probability of entangling larger numbers of photons becomes very small. (Nevertheless, by waiting long enough, three-photon entangled states were recently observed from simultaneous downconversion into two pairs [18]). Experiments in cavity-QED have recently shown entanglement of two atoms [19] and two atoms with a photon [20], where atoms from a thermal (random) source traverse a common microwave cavity. In these experiments, $\epsilon \simeq 0.005$. Experiments with

optical parametric oscillators can also entangle the continuous quadratures of two optical field modes [21]. Although this source has near-unit entanglement efficiency, scaling to larger numbers of degrees of freedom appears difficult.

The Cirac-Zoller Scheme

In 1995, Cirac and Zoller showed that a collection of trapped ions may be suitable for storing large-scale entangled states such as $|\Psi_{QC}\rangle$ [22]. In their proposal, each atomic ion stores a quantum bit (qubit) of information in a pair of electronic energy levels, and a collective mode of harmonic vibration is used to entangle any pair of ion qubits. By applying laser beams to an individual ion in the collection, its internal qubit state can be mapped onto the collective ion motion, and subsequent quantum logic gates can be applied between the motion and a second ion, effectively entangling the two ions. The entanglement can be extended to any number of ions by repeating these steps on other pairs of ions. When accompanied by single-ion rotations, the Cirac-Zoller scheme allows the creation of an arbitrary entangled state [Eq. (2)], and therefore forms a set of universal quantum logic gates.

The basic elements of the Cirac-Zoller scheme were demonstrated on a single trapped ion in 1995 [23]. A variation of this scheme was later used to entangle a pair of trapped ions [24] with entanglement efficiency $\epsilon \simeq 0.8$, representing the first scalable entanglement source with near-unit efficiency.

The Mølmer-Sørensen Scheme

Instead of entangling the ions sequentially, Mølmer and Sørensen showed how to create the N-ion entangled state

$$|\Psi_N\rangle = \frac{|\uparrow\rangle_1|\uparrow\rangle_2\cdots|\uparrow\rangle_N + e^{i\phi_N}|\downarrow\rangle_1|\downarrow\rangle_2\cdots|\downarrow\rangle_N}{\sqrt{2}} \qquad (3)$$

with a single pulse of laser radiation [25]. The Mølmer-Sørensen operation applied to any pair of qubits in a collection of ions (accompanied by single ion rotations) allows the creation of any entangled state [Eq. (2)], and thus forms a set of universal quantum logic gates alternative to the Cirac-Zoller scheme [26]. We have employed the Mølmer-Sørensen scheme to create the entangled state of Eq. (3) for $N = 2$ and $N = 4$ trapped ions [27]. In both cases, the entanglement efficiency was $\epsilon \simeq 0.8$, as discussed below.

The Mølmer-Sørensen entanglement technique can be understood by considering a pair of identical spin-1/2 charged particles confined together in a harmonic potential [28]. The energy levels of this system are illustrated in Fig. 1, where $\hbar\omega_0$ is the internal energy splitting of each qubit, and ν is the oscillation frequency of a particular collective mode of the particles in the trap.
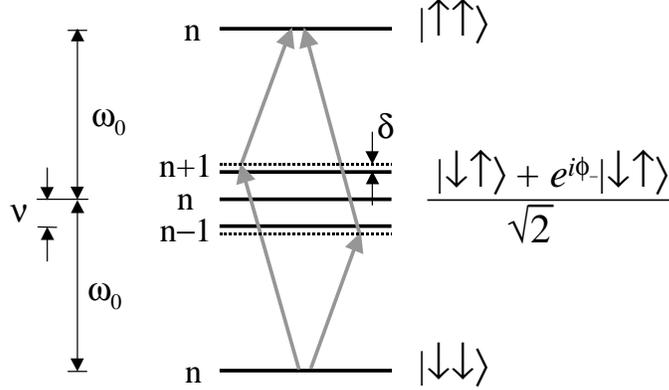
FIGURE 1. Entanglement scheme for two particles. Each ion is prepared initially in the $|\downarrow\downarrow\rangle$ internal state, and the collective motion of the pair contains exactly n quanta. Laser fields equally illuminating the two ions and oscillating near $\omega_0 + \nu + \delta$ and $\omega_0 - \nu - \delta$ couple the $|\downarrow\downarrow\rangle$ and $|\uparrow\uparrow\rangle$ states as shown. For sufficient detuning δ, the populations of the middle states are kept small. By driving the double transition for the appropriate period, the entangled state $(|\uparrow\uparrow\rangle + e^{i\phi_2}|\downarrow\downarrow\rangle)/\sqrt{2}$ is generated. For four ions, the same procedure generates the state $(|\uparrow\uparrow\uparrow\uparrow\rangle + e^{i\phi_4}|\downarrow\downarrow\downarrow\downarrow\rangle)/\sqrt{2}$.

The ions are prepared initially in the $|\downarrow\downarrow\rangle$ internal state, and we assume the ions are in a collective motional eigenstate $|n\rangle$. By simultaneously applying optical fields near the first upper and lower motional sidebands (oscillating at $\omega_0 + \nu + \delta$ and $\omega_0 - \nu - \delta$ respectively) with equal illumination on the two ions, the two-step transition from $|\downarrow\downarrow\rangle|n\rangle$ to $|\uparrow\uparrow\rangle|n\rangle$ is driven through the intermediate states

$$|\Psi_{int}\rangle_\pm = \frac{|\downarrow\rangle|\uparrow\rangle|n\pm 1\rangle + e^{i\phi_-}|\uparrow\rangle|\downarrow\rangle|n\pm 1\rangle}{\sqrt{2}}, \tag{4}$$

where ϕ_- is the phase difference of the field at the two ion positions. For sufficiently large detuning δ from the sidebands, these intermediate states are negligibly occupied, so that the motional state is not altered. We also assume $\delta \ll \nu$ so that intermediate states involving other motional modes are not involved in the coupling. As shown in Fig. 1, there are two paths from $|\downarrow\downarrow\rangle$ to $|\uparrow\uparrow\rangle$, and their respective couplings are given by the product of the two resonant sideband Rabi frequencies divided by the detuning $\pm\delta$ from the relevant virtual intermediate level. For the upper- then lower-sideband path (arrows on left side of Fig. 1), this coupling is $(\eta g\sqrt{n+1})^2/\delta$, and for the lower- then upper-sideband path (arrows on right side of Fig. 1), it is $-(\eta g\sqrt{n})^2/\delta$, where g is the single ion resonant carrier Rabi frequency and η is the Lamb-Dicke parameter of the motional mode involved. (These expressions are valid only in the Lamb-Dicke limit $\eta^2(n+1) \ll 1$.) Adding the couplings from these two paths results in a net Rabi frequency from $|\downarrow\downarrow\rangle$ to $|\uparrow\uparrow\rangle$ of $\Omega = \eta^2 g^2/\delta$, independent of the motional state $|n\rangle$ within the Lamb-Dicke regime. The net interaction Hamiltonian is proportional to $\sigma_x^{(1)}\sigma_x^{(2)}$, where $\sigma_x^{(i)}$ is the transverse Pauli spin-1/2 operator of ion i. Entanglement is achieved by simply applying these beams for a period $\tau = \pi/2\Omega$, creating the desired spin state

$$|\Psi_2\rangle = \frac{|\uparrow\uparrow\rangle + e^{i\phi_+}|\downarrow\downarrow\rangle}{\sqrt{2}}, \tag{5}$$

where ϕ_- is the sum of the field phases at the two ion positions.

1   Fast Entanglement

In order for the intermediate states $|\Psi_{int}\rangle_\pm$ to be negligibly occupied, the detuning δ must be large compared to both single-spin sideband Rabi frequencies $\eta g\sqrt{n+1}$ and $\eta g\sqrt{n}$, meaning the entangling operation must be much slower than the resonant sideband operations. (This is the characteristic slowdown of driving higher-order transitions through virtual levels.) However, it is possible to violate this condition and still generate the state $|\Psi_2\rangle$ [29,30]. In this case, the intermediate states $|\Psi_{int}\rangle_\pm$ are occupied during the operation (and the motional state becomes entangled with the spins), but this occupation can vanish at exactly the moment at which the desired entangled spin state $|\Psi_2\rangle$ is created. Without regard to the the spin states, we find that for arbitrarily small δ (and within the Lamb-Dicke limit), the motion evolves during the operation as a coherent superposition of its original state $\rho_m(0)$ and an oscillating displaced state [29]

$$\rho_m^{dis}(t) = \mathcal{D}\left[\sqrt{\frac{\Omega}{\delta}}(e^{i\delta t} - 1)\right] \rho_m(0) \mathcal{D}\left[\sqrt{\frac{\Omega}{\delta}}(e^{i\delta t} - 1)\right]^\dagger, \tag{6}$$

where $\mathcal{D}(\alpha)$ is the displacement operator with phase space argument α [31]. The overall motion is thus in a "Schrödinger Cat"-type superposition state [32], with maximum separation in phase space $2\sqrt{\Omega/\delta}$. The phase space trajectory of the displaced component $\rho_m^{dis}(t)$ follows a circle from its original state with radius $\sqrt{\Omega/\delta}$, returning to the initial motional state $\rho_m(0)$ at times $t_m = 2\pi m/\delta$, where the positive integer m is the number of complete circular cycles of the displacement [29]. Setting the entanglement pulse period τ defined above equal to t_m, we find that the condition for a return to the initial motional state following the entanglement step is $\Omega/\delta = 1/(4m)$. The entangling peiod can thus be rewritten as $\tau = \pi\sqrt{m}/(\eta g)$, which is only a factor of $2\sqrt{m}$ longer than an analogous resonant sideband transition. To maximize the speed of the Mølmer-Sørensen operation in the experiment, we operate with $m = 1$.

2   Scalable Entanglement

Surprisingly, the Mølmer-Sørensen entangling scheme is scalable in the sense that precisely the same operation can be used to generate the N-particle entangled state of Eq. (3) for any even number N of ions. (For N odd, $|\Psi_N\rangle$ can be generated using one entanglement pulse accompanied by a separate independent rotation of

each particle's spin.) The Mølmer-Sørensen interaction is proportional to J_x^2, where J_x is the transverse spin operator for the effective spin-$N/2$ particle. Physically, this interaction simultaneously flips all pairs of ions in the collection. Through the properties of angular momentum rotations [25], this results in the desired entangled state $|\Psi_N\rangle$. In scaling to larger numbers of ions, the only difference (for a given motional mode frequency) is that the operation is $\sqrt{N}$ times slower, since the Lamb-Dicke parameter is proportional to $1/\sqrt{N}$. In addition, the phase which appears in Eq. (3) is the sum of the field phases at each ion position.

If the ions are uniformly illuminated, the Mølmer-Sørensen scheme requires that they all participate equally in the intermediate motional excitation, which implies that the only suitable mode for arbitrary N is the center-of-mass mode. However, this mode has a practical disadvantage that fluctuating ambient electric fields cause it to heat at a significant rate [33]. For large δ, the entanglement operation is independent of the motion, so that heating is unimportant so long as the ions remain in the Lamb-Dicke regime [29]. In the small-δ case, however, motional decoherence of the Schrödinger-Cat state discussed above must be avoided. Modes involving only relative ion motion couple to higher moments of the field, so heating of them is negligible [34]. For $N = 2$ and $N = 4$ ions, such modes do exist in which each particle participates with equal amplitude [35]. In both cases, they are uniform "stretch" modes, in which alternating ions oscillate out of phase; we use these modes here. Excitation of the center-of-mass mode does still affect the experiment, as the ion can eventually get heated out of the Lamb-Dicke regime. For this reason, we initially sideband cool both the center-of-mass and uniform stretch modes to near their ground state. We note that other modes of motion can also be used for entanglement, as long as the laser intensity on each ion is adjusted to compensate for the difference in mode amplitude of that ion, resulting in equal sideband couplings for all ions.

EXPERIMENT

The experiment was performed using $^9\text{Be}^+$ ions confined in a miniature linear RF trap [33], with the N ions lying in a line along the trap's weak axis. Two spectrally resolved ground-state hyperfine levels compose the effective spin-1/2 system, with $|\downarrow\rangle \equiv |F = 2, m_F = -2\rangle$, $|\uparrow\rangle \equiv |F = 1, m_F = -1\rangle$. The hyperfine splitting between these states is $\omega_0/2\pi \simeq 1.25$ GHz.

Coherent coupling between $|\downarrow\rangle$ and $|\uparrow\rangle$ is provided via stimulated Raman transitions. The two Raman laser beams have a wavelength of $\lambda \simeq 313$ nm, with a difference frequency near ω_0. Their wavevectors are perpendicular, with their difference wavevector lying along the line of ions with magnitude $\delta k = 2\pi\sqrt{2}/\lambda$. They are detuned ~ 80 GHz blue of the $2P_{1/2}$ excited state, with intensities giving $g/2\pi \simeq 500$ kHz.

The Raman beam frequencies can also be tuned to coherently flip the spins while simultaneously affecting the collective motional state of the ions. For modes con-

sidered here (having equal amplitudes of motion for all the ions), the spin-motional coupling is determined by the Lamb-Dicke parameter $\eta = \delta k(\hbar/2Nm_1\nu)^{1/2}$ of the mode with frequency ν, where m_1 is the mass of a single particle in the collection.

Fig. 2 displays a stimulated-Raman absorption spectrum of four trapped ions in a linear array, with the four axial modes as well as higher-order features clearly visible. For both the two- and four-ion experiments, the desired stretch-mode frequency was set to $\nu/2\pi \simeq 8.8$ MHz, giving a Lamb-Dicke parameter of $\eta_{STR} = 0.23/N^{1/2}$. For the Mølmer-Sørensen operation, the two driving frequencies required to generate a coupling near the first blue- and first red-sidebands are generated by frequency modulating one of the Raman beams using an electro-optic modulator. The spectral positions of the relevant difference frequencies of the Raman beam pairs are indicated by the two arrows and dashed vertical lines in Fig. 2.
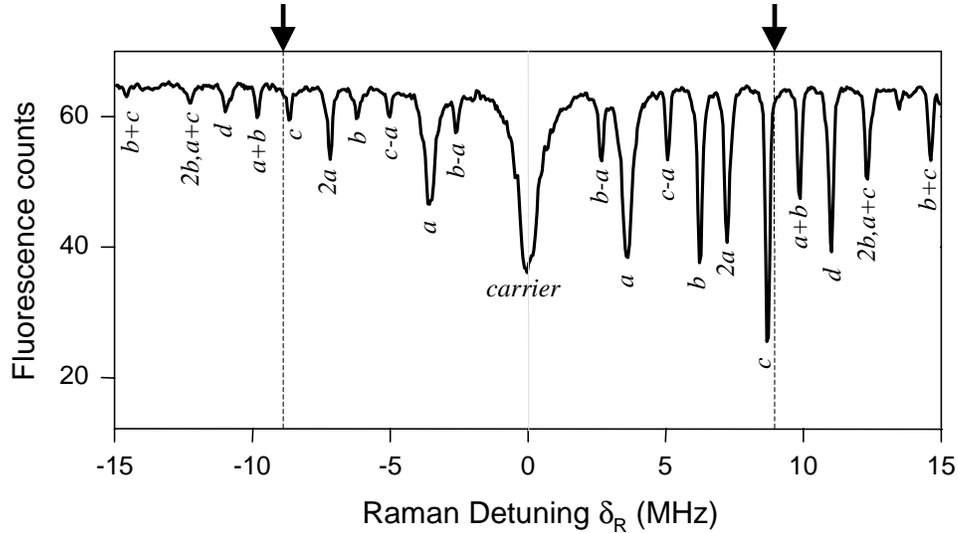

FIGURE 2. Raman absorption spectrum of four ions confined in a linear crystal and Doppler laser-cooled. The ordinate is the detuning δ_R of the Raman beams' difference frequency from the carrier, and the abscissa shows the average counts of ion fluorescence per experiment (200 μs integration time), proportional to the number of ions in the state $|\downarrow\rangle$ (the ions are initially prepared in state $|\downarrow\downarrow\downarrow\downarrow\rangle$). The carrier appears at $\delta_R = 0$, and the first sidebands of the four axial normal modes of motion (labelled by letters a-d) appear at $\delta_R = \pm 3.62, \pm 6.23, \pm 8.67$ MHz, and ± 11.02 MHz, in agreement with the theoretical frequency ratios $1 : \sqrt{3} : 2.410 : 3.051$. Several higher-order sidebands also appear at sums and differences of harmonics of the normal-mode frequencies, as indicated. The sideband asymmetry (upper sidebands are stronger) indicates cooling to the quantum regime with only a few thermal phonons. The two arrows and the dashed lines, just outside the first upper and lower stretch sidebands, indicate the frequencies used for the four-ion Mølmer-Sørensen scheme.

After an interaction with the stimulated Raman beams, the ions' internal states are measured by illuminating them with a circularly polarized laser beam tuned to the $2S_{1/2}(F = 2, m_F = -2) \leftrightarrow 2P_{3/2}(F = 3, m_F = -3)$ cycling transition. Each

TABLE 1. Characterization of two-ion and four-ion states. P_j denotes the probability that j ions were measured to be in $|\downarrow\rangle$, and $|\rho_{\uparrow...\uparrow,\downarrow...\downarrow}|$ denotes the coherence between $|\uparrow...\uparrow\rangle$ and $|\downarrow...\downarrow\rangle$. Uncertainties in the $N = 2$ measurements are ±0.01; uncertainties in the $N = 4$ populations are ±0.02.

N	P_0	P_1	P_2	P_3	P_4	$|\rho_{\uparrow...\uparrow,\downarrow...\downarrow}|$
2	0.43	0.11	0.46	-	-	0.385
4	0.35	0.10	0.10	0.10	0.35	0.215

ion in $|\downarrow\rangle$ fluoresces brightly, leading to the detection of $\sim$15 photons/ion on a photomultiplier tube after a 200 μs detection period. In contrast, an ion in $|\uparrow\rangle$ remains nearly dark. For a single ion, we are able to discriminate between $|\uparrow\rangle$ and $|\downarrow\rangle$ with approximately 99% accuracy, as shown in the histograms of Figs. 3a and 3b. This accuracy is limited by off-resonant optical pumping, which causes the dark state $|\downarrow\rangle$ to eventually partake in the cycling transition and fluoresce [24]. This error rate of 1% could be improved considerably by appropriately weighting the photon counts by their arrival time, as this optical pumping will contaminate later counts more so than earlier counts. Fig. 3c shows a histogram of four ions prepared in an initial state with incoherent populations in all five possible states of excitation without distinguishing the individual ions. Here, the number of ions in state $|\downarrow\rangle$ can be determined with an accuracy of about 80% on any a given experiment, although this number could be improved to better than 95% by weighting the counts as discussed above. These statistical detection errors can be averaged away by repeating the experiment many times and fitting the resulting photon-number distribution to a sum of Poissonians to determine the probability distribution P_j of having exactly j ions in the state $|\downarrow\rangle$ [24].

N-particle entanglement results

Following the Mølmer-Sørensen entangling procedure, the probability distribution P_j is measured. The results are given in Table 1, and show that in both cases, the probabilities for all N ions to be in the same state are large compared to the probabilities for the other cases. This is characteristic of the state $|\Psi_N\rangle$ [Eq. (3)], although the fact that the middle probabilities are nonzero indicates that we do not generate the entangled states with perfect accuracy.

In order to prove that we are generating a reasonable approximation to $|\Psi_N\rangle$, it is necessary to prove that the populations of $|\uparrow\uparrow\uparrow\uparrow\rangle$ and $|\downarrow\downarrow\downarrow\downarrow\rangle$ are coherent. In terms of the N-spin density matrix ρ_N, we must measure the far off-diagonal element $\rho_{\uparrow...\uparrow,\downarrow...\downarrow}$. This can be achieved by viewing the first entanglement pulse as the first pulse in a Ramsey experiment [36], and applying a second (non-entangling)
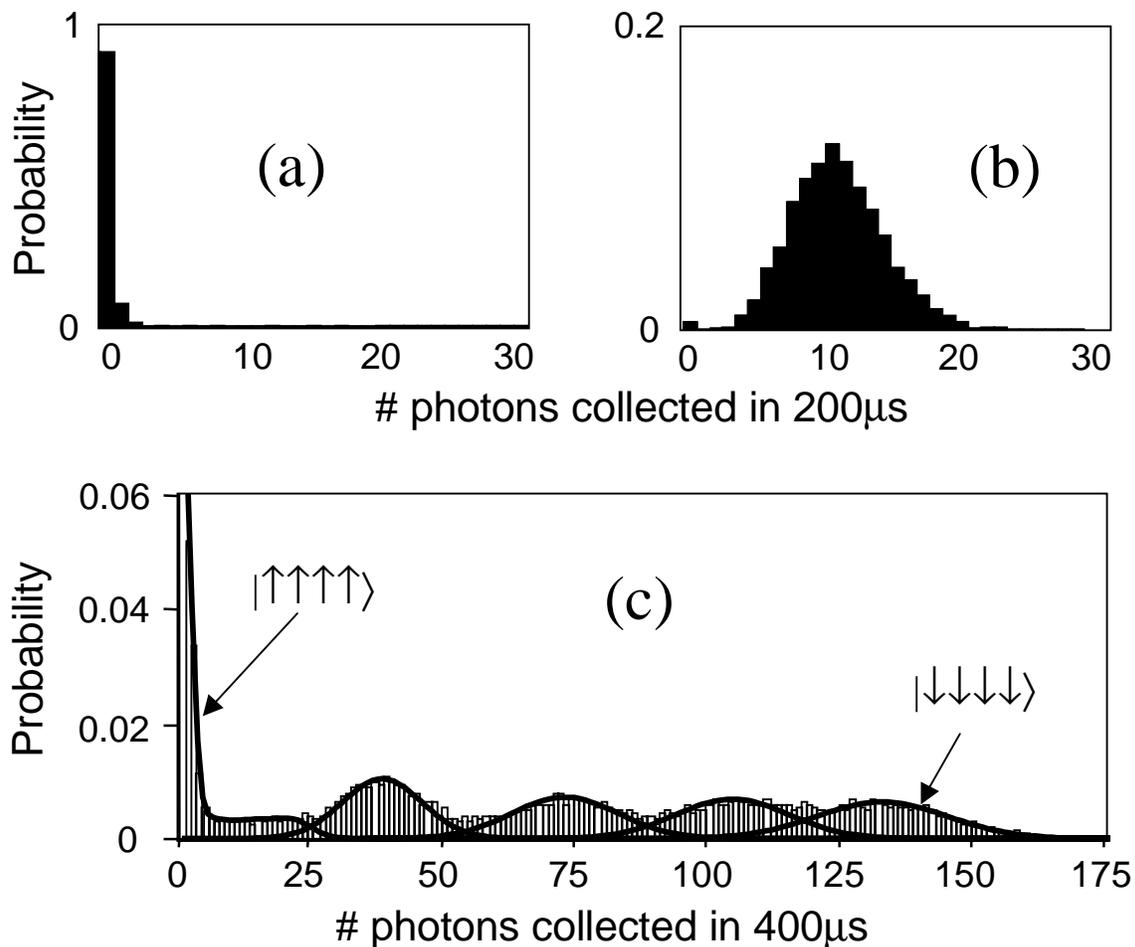
FIGURE 3. Measured probability distribution of detected fluorescence counts of a single trapped ion in (a) state $|\uparrow\rangle$ and (b) state $|\downarrow\rangle$ after 200 μs of integration (1000 measurements). (c) Measured probability distribution of detected fluorescence counts of four trapped ions after 400 μs of integration (1000 measurements). The lines are least-squares fits to reference distributions for having anywhere from 0 ions (leftmost curve) to 4 ions (rightmost curve) in state $|\downarrow\rangle$, providing relative probabilities P_j of j ions in state $|\downarrow\rangle$.

$\pi/2$ pulse to the ions before observing them, closing the Ramsey interferometer. The relevant observable after this modified Ramsey experiment is the parity of the number of ions in state $|\downarrow\rangle$ [37]

$$\Pi(\phi) \equiv \sum_{j=0}^{N}(-1)^j P_j(\phi). \tag{7}$$

As the parity is measured while ϕ is varied, the resulting Ramsey fringes oscillate as $\cos N\phi$ for N ions, as seen in Fig. 4. The amplitude of the fringes is just twice the desired coherence $2|\rho_{\uparrow...\uparrow,\downarrow...\downarrow}|$. This compression of the Ramsey fringes by a factor
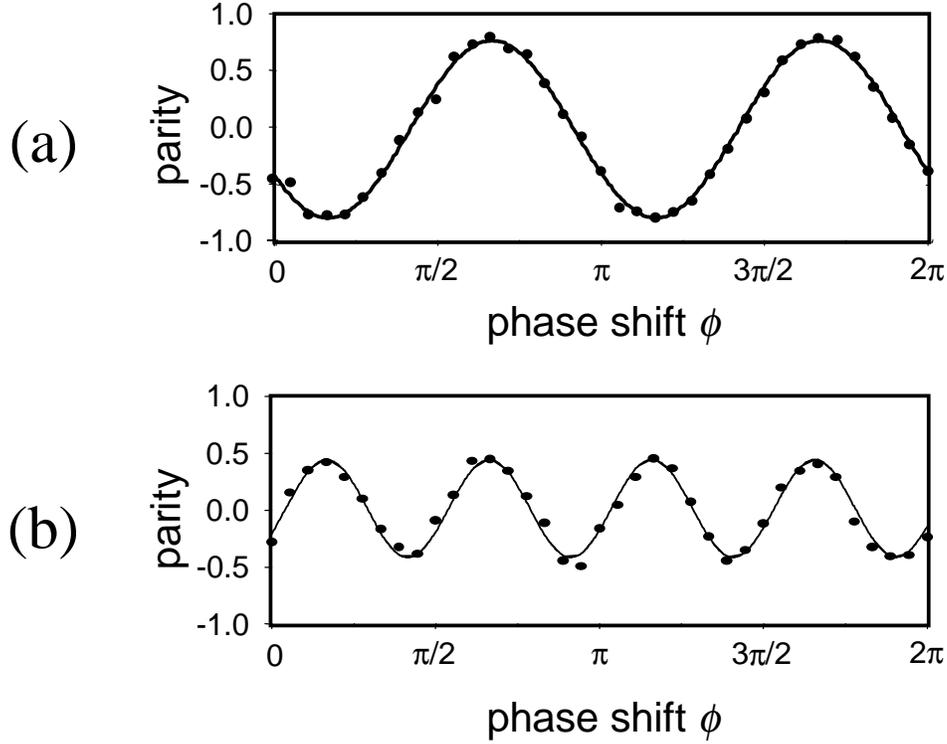
FIGURE 4. Determination of $\rho_{\uparrow\ldots\uparrow,\downarrow\ldots\downarrow}$ for (a) two ions and (b) four ions. After the entanglement operation, a non-entanling $\pi/2$ pulse with relative phase ϕ drives the $|\downarrow\rangle \leftrightarrow |\uparrow\rangle$ transition in each ion. As ϕ is varied, the parity of the N ions oscillates as $\cos N\phi$, and the amplitude of the oscillation is twice the magnitude of the density-matrix element $\rho_{\uparrow\ldots\uparrow,\downarrow\ldots\downarrow}$. Each data point represents an average of 1000 experiments, corresponding to a total integration time of roughly 10 s for each graph.

of N is the basis for extracting Heisenberg-limited signal-to-noise in spectroscopy of entangled states, where the frequency uncertainty $\Delta\omega$ is limited by the N-particle Heisenberg uncertainty relation $\Delta\omega\Delta t \geq 1/N$ for observation time Δt [37]. Fig. 5 shows an analog of this effect in a Mach-Zender interferomer.

The measurements of $|\rho_{\uparrow\ldots\uparrow,\downarrow\ldots\downarrow}|$ are listed in the last column of Table 1 for both 2- and 4-ion cases. The fidelity of our state generation, or the overlap between the idealized state $|\Psi_N\rangle$ in Eq. (3) and the observed density matrix, is

$$\mathcal{F}_N \equiv \langle|\Psi_N\rangle|\rho_N|\Psi_N\rangle = \frac{P_0 + P_N}{2} + |\rho_{\uparrow\ldots\uparrow,\downarrow\ldots\downarrow}|. \tag{8}$$

For $N = 2$ we achieve $\mathcal{F}_2 = 0.83 \pm 0.01$, while for $N = 4$, $\mathcal{F}_4 = 0.57 \pm 0.02$. In both cases the fidelity is above 0.5, indicating N-particle entanglement [27].

Quantifying the *amount* of entanglement is a more difficult question. A variety of measures of entanglement have been proposed, but most are difficult to calculate even numerically [38,39]. For $N = 2$, Wootters has given an explicit formula for
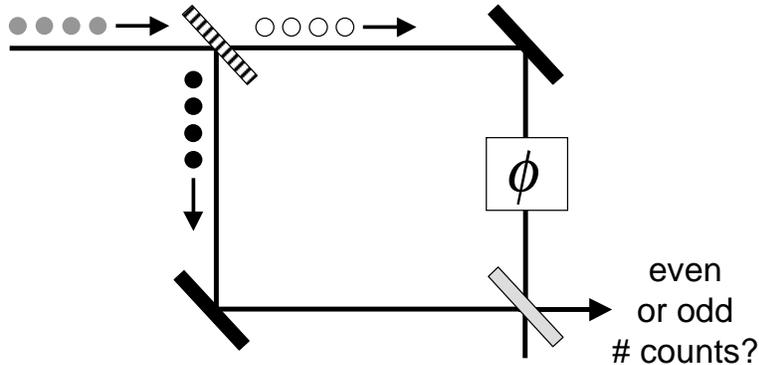
FIGURE 5. Mach-Zender interferometer analog for four-particle entanglement observation. Four photons propagate through a "super-beamsplitter," which sends the photons in a superposition of all going through and all reflecting. One arm contains a phase shifter, and the two paths are recombined on a normal beamsplitter. The parity of the number of photons received in one of the output ports is measured as the interferometer phase is scanned. Because the photons all take the same path, the measured phase shift is amplified by a factor of four (fringe period $= \pi/2$), providing enhanced interferometric sensitivity.

the *entanglement of formation*, $\mathcal{E}(\rho_2)$ [40]. Although we have not reconstructed the entire two-particle density matrix, the populations measured place sufficient bounds on the unmeasured elements to determine that $\mathcal{E}(\rho_2) \approx 0.5$. This indicates that roughly two pairs of our ions would be required to carry the same quantum information as a single perfectly entangled pair.

In the four-ion case, no explicit formula for entanglement is known. The data does indicate that our density matrix can be expressed as

$$\rho_4 \simeq 0.43|\Psi_4\rangle\langle\Psi_4| + 0.57\rho_4^{incoh}, \tag{9}$$

where $|\Psi_4\rangle$ is the desired state of Eq. (3) and ρ_4^{incoh} is completely incoherent (ie., diagonal). The coefficients of Eq. (9) are determined directly from the value of $\rho_{\uparrow\uparrow\uparrow\uparrow,\downarrow\downarrow\downarrow\downarrow}$ in Table I, together with the fact that no evidence for other off-diagonal matrix elements was observed. (Other coherences involving less than four ions would have given fringes varying as $cos\phi$, $cos2\phi$, or $cos3\phi$ in the measured populations $P_j(\phi)$ and parity $\Pi(\phi)$).

A measurement of $|\rho_{\uparrow...\uparrow,\downarrow...\downarrow}| > 0$ does not by itself guarantee N-particle entanglement. For instance, consider the four-particle states

$$|\Psi_A\rangle = \left(\frac{|\downarrow\downarrow\downarrow\rangle + |\uparrow\uparrow\uparrow\rangle}{\sqrt{2}}\right) \otimes \left(\frac{|\downarrow\rangle + |\uparrow\rangle}{\sqrt{2}}\right) \tag{10}$$

and

$$|\Psi_B\rangle = \left(\frac{|\downarrow\downarrow\downarrow\rangle + i|\uparrow\uparrow\uparrow\rangle}{\sqrt{2}}\right) \otimes \left(\frac{|\downarrow\rangle - i|\uparrow\rangle}{\sqrt{2}}\right). \tag{11}$$

An equally weighted statistical mixture of Ψ_A and Ψ_B exhibits only three-particle entanglement, yet has $|\rho_{\uparrow...\uparrow,\downarrow...\downarrow}| = 0.25$ (larger than our observed value) without any other coherences. A similar mixed state with pairs of two-particle entangled states also has $|\rho_{\uparrow...\uparrow,\downarrow...\downarrow}| = 0.25$ without other coherences. However, these states significantly differ from $|\Psi_4\rangle\langle\Psi_4|$ along the density matrix diagonals, so the observed populations P_j following the entanglement procedure (Table 1) can set an upper bound on how much these states can contribute to the measured density matrix. We decompose ρ_4 as a sum of the desired state $|\Psi_4\rangle\langle\Psi_4|$ and a "worst-case" factorizable density matrix ρ_4^F that includes mixed states such as above. We find that an upper bound on the amount of four-particle coherence in ρ_4^F is

$$\rho_{\uparrow\uparrow\uparrow\uparrow,\downarrow\downarrow\downarrow\downarrow}^F(max) = Min\left[P_0, P_4, \frac{P_2}{2} + Min(P_1, P_3)\right]. \tag{12}$$

¿From the data in Table (1), we find that $\rho_{\uparrow\uparrow\uparrow\uparrow,\downarrow\downarrow\downarrow\downarrow}^F(max) = 0.15$, leaving the remainder of the observed four-particle coherence (0.065) to be unambiguously associated with the four-particle entangled state $|\Psi_4\rangle$. This gives the worst-case decomposition

$$\rho_4 = 0.13|\psi_4\rangle\langle\psi_4| + 0.87\rho_4^F, \tag{13}$$

where ρ_4^F contains mixtures of particular two- and three-particle entangled states (such as Eqs. (10) and (11)) that are very unlikely to occur in the experiment.

OUTLOOK

The data on two-ion and four-ion entanglement are consistent with an entanglement efficiency of $\epsilon \approx 0.8$. Although this represents the only demonstrated source of 4-particle entanglement and uses a scalable method, the imperfect contrast of (Fig. 4) indicates that even this efficiency will limit how many particles can be entangled in this experiment. It may be required to achieve entanglement efficiencies $\epsilon > 0.9999$ in order to implement fault-tolerant error correction schemes which may allow entanglement of arbitrarily large numbers of particles [41].

Several technical noise sources degrade the observed efficiency, including laser intensity and beam-pointing noise, nonuniform illumination of the ions during the Mølmer-Sørensen operation, and magnetic field noise. The chief limitation in the current experiment appears to be stochastic heating of the ions to outside the Lamb-Dicke regime. The center-of-mass (CM) motion of the ions is observed to heat at a rate of $\langle\dot{n}_{CM}\rangle \approx 0.02N$ μs^{-1} [33], so after a 10 μs four-ion entangling operation, $\langle n_{CM}\rangle$ approaches ≈ 10 thermal quanta. This invalidates the Lamb-Dicke criterion $\eta_{CM}^2\langle n_{CM}\rangle \ll 1$, and severely limits the fidelity of the operation. Mølmer and Sørensen have shown [29] that the expected fidelity of the entangled state $|\Psi_N\rangle$ of N ions is

$$\mathcal{F} \approx 1 - N(N-1)\eta_{CM}^4\langle n_{CM}\rangle^2, \tag{14}$$

to lowest order in the center-of-mass Lamb-Dicke parameter η_{CM} with $N \gg 1$ and $\langle n_{CM} \rangle \gg 1$. The factor $N(N-1)/2$ comes from the number of pairs of N ions that are simultaneously flipped during the Mølmer-Sørensen entangling operation. We find that for the $N = 4$ experiment, the above expression is consistent with the observations.

The source of ion heating has not been pinpointed, but it appears to be related to fluctuating microscopic potentials on the electrodes. The observed heating is not a fundamental limitation, as it has been observed to be orders of magnitude smaller under some conditions [33]. Moreover, by trapping multiple ion species and continuously laser-cooling one, the other qubit ions can be sympathetically cooled to remain in the Lamb-Dicke regime while not disturbing the qubit coherence [42].

Producing entangled states of very large numbers of ions (tens or hundreds) for relevance to large-scale quantum computing will require a different approach. This is because a trap confining more than several ions will likely have lower oscillation frequencies, and mode cross-coupling from the complicated mode structure will be unavoidable. A promising path to large numbers is to use a multiplexed ion trap structure of many separated ion traps [43]. Here, entangling operations are done only in traps holding a few $(2-5)$ ions, and the ions are be shuttled between traps to extend the entanglement to larger numbers. Because the quantum bits are stored in magnetic dipole (hyperfine) internal states and the ions are moved around with electric fields acting on their charge, the coherence of the qubits should not be disturbed. Peeling away an ion from, or introducing an ion to, other ions in a trap will obviously introduce a significant amount of motional energy, but this energy can be removed again by trapping multiple species and relying on sympatheic cooling to return the motion to well inside the Lamb-Dicke regime for subsequent entangling operations.

REFERENCES

1. D. Bohm, *Quantum theory* (Prentice Hall, Engelwood Cliffs, NJ, 1951).
2. A. Einstein, B. Podolsky, and N. Rosen, Phys. Rev. **47**, 777 (1935).
3. J. S. Bell, Physics **1**, 195 (1964).
4. C. H. Bennett and S. J. Weisner, Phys. Rev. Lett. **69**, 2881 (1996).
5. K. Mattle, H. Weinfurter, P. G. Kwiat, and A. Zeilinger, Phys. Rev. Lett. **76**, 4656 (1996).
6. A. K. Ekert, Phys. Rev. Lett. **67**, 661 (1991).
7. C. H. Bennett *et al.*, Phys. Rev. Lett. **70**, 1895 (1993).
8. D. Bouwmeester *et al.*, Nature **390**, 575 (1997).
9. D. Boschi *et al.*, Phys. Rev. Lett. **80**, 1121 (1998).
10. A. Furusawa *et al.*, Science **282**, 706 (1998).
11. P. W. Shor, *Proceedings of the 35th Annual Symposium on the Foundations of Computer Science* (IEEE Computer Society Press, New York, 1994), p. 124.
12. L. K. Grover, Phys. Rev. Lett. **79**, 325 (1997).
13. A. M. Steane and D. M. Lucas, quant-ph/0004053 (2000).

14. S. J. Freedman and J. F. Clauser, Phys. Rev. Lett. **28**, 938 (1972).
15. A. Aspect, P. Grangier, and G. Roger, Phys. Rev. Lett. **49**, 91 (1982).
16. Z. Y. Ou and L. Mandel, Phys. Rev. Lett. **61**, 50 (1988).
17. Y. H. Shih and C. O. Alley, Phys. Rev. Lett. **61**, 2921 (1988).
18. D. Bouwmeester *et al.*, Phys. Rev. Lett. **82**, 1345 (1999).
19. E. Hagley *et al.*, Phys. Rev. Lett. **79**, 1 (1997).
20. A. Rauschenbeutel *et al.*, Science **288**, 2024 (2000).
21. Z. Y. Ou, S. F. Pereira, H. J. Kimble, and K. C. Peng, Phys. Rev. Lett. **68**, 3663 (1992).
22. J. I. Cirac and P. Zoller, Phys. Rev. Lett. **74**, 4091 (1995).
23. C. Monroe *et al.*, Phys. Rev. Lett. **75**, 4714 (1995).
24. Q. A. Turchette *et al.*, Phys. Rev. Lett. **81**, 1525 (1998).
25. K. Mølmer and A. Sørensen, Phys. Rev. Lett. **82**, 1835 (1999).
26. K. Mølmer and A. Sørensen, Phys. Rev. Lett. **82**, 1971 (1999).
27. C. A. Sackett *et al.*, Nature **404**, 256 (2000).
28. E. Solano, R. L. de Matos Filho, and N. Zagury, Phys. Rev. A **59**, 2539 (1999).
29. A. Sørensen and K. Mølmer, quant-ph/0002024 (2000).
30. G. J. Milburn, quant-ph/9908037 (1999).
31. D. F. Walls and G. J. Milburn, *Quantum Optics* (Springer Verlag, Berlin, 1994).
32. C. Monroe, D. M. Meekhof, B. E. King, and D. J. Wineland, Science **272**, 1131 (1996).
33. Q. A. Turchette *et al.*, Phys. Rev. A **61**, 063418 (2000).
34. B. E. King *et al.*, Phys. Rev. Lett. **81**, 1525 (1998).
35. D. James, Appl. Phys. B **66**, 181 (1998).
36. N. F. Ramsey, *Molecular Beams* (Oxford University Press, London, 1963).
37. J. J. Bollinger, W. M. Itano, D. J. Wineland, and D. J. Heinzen, Phys. Rev. A **54**, R4649 (1996).
38. V. Vedral, M. Plenio, M. Rippin, and P. Knight, Phys. Rev. Lett. **78**, 2275 (1997).
39. M. Lewenstein and A. Sanpera, Phys. Rev. Lett. **80**, 2261 (1998).
40. W. K. Wootters, Phys. Rev. Lett. **80**, 2245 (1998).
41. W. H. Zurek, Physics Today **52**, 24 (1999).
42. D. Kielpinski *et al.*, Phys. Rev. A **61**, 032310 (2000).
43. D. J. Wineland *et al.*, J. Res. Nat. Inst. Stand. Tech. **103**, 259 (1998).